Hindawi
Journal of Spectroscopy
Volume 2024, Article ID 6693346, 9 pages
https://doi.org/10.1155/2024/6693346

Research Article

Gemological and Spectral Characteristics of Gem-Quality Blue Gahnite from Nigeria

Yifang Chen,[1,2] **Junhao Zheng**,[1,2] **Mingmei Lu**,[1,2] **Ziqi Liu**,[1,2] **and Zhengyu Zhou**[1,2,3]

[1]*The State Key Laboratory of Marine Geology, Tongji University, Shanghai 200092, China*
[2]*Ocean and Earth Science School, Tongji University, Shanghai 200092, China*
[3]*Laboratory of Gem and Technological Materials, Tongji University, Shanghai 200092, China*

Correspondence should be addressed to Zhengyu Zhou; 06058@tongji.edu.cn

Received 13 September 2023; Revised 12 December 2023; Accepted 30 January 2024; Published 10 February 2024

Academic Editor: Mohd Sajid Ali

Gem-quality blue octahedral crystalline gahnite was produced in Nigeria. This paper investigated gemological and spectroscopic characteristics by basic gemological experiments, electron probes, infrared reflectance spectroscopy, laser Raman spectroscopy, photoluminescence spectroscopy, and ultraviolet-visible spectroscopy. The results show that the refractive index (RI) of Nigerian gahnite is 1.792~1.794, and the specific gravity is 4.45~4.66, with no fluorescence. The main chemical composition is $ZnAl_2O_4$, accounting for 93.57%, and the rest is mainly $FeAl_2O_4$, which also contains Na, Mg, Co, Mn, Cr, Cu, Si, K, and Ca elements. The infrared spectra showed midinfrared absorption bands near 510 cm^{-1}, 559 cm^{-1}, and 664 cm^{-1} in the fingerprint region, corresponding to the Zn-O stretching vibration, bending vibration, and Al-O bending vibration, respectively. The Raman spectra showed three of the five Raman active modes of the spinel group, with characteristic Raman absorption peaks located at 418 cm^{-1}, 508 cm^{-1}, and 660 cm^{-1}, corresponding to E_g, $T_{2g(2)}$, and $T_{2g(3)}$ modes, respectively, and the comparison revealed a higher degree of Zn and Al ordering in this paper for gahnite. The photoluminescence spectra show the common Cr^{3+}-activated fluorescence splitting peaks of natural spinel, of which the 686 nm (R-line) fluorescence peak is obvious and sharp. The UV-vis absorption spectra located at 444 nm and 489 nm are the most obvious, which are caused by the *d-d* electron leap of ${}^{T}Fe^{2+}$ (${}^{5}E \longrightarrow {}^{5}T_2$), and the blue-gray tones of the samples are mainly caused by the spin-forbidden electronic transitions in ${}^{T}Fe^{2+}$ and ${}^{M}Fe^{2+} \leftrightarrow {}^{M}Fe^{3+}$; the weak absorption peak at 609 nm was determined to be associated with Co^{2+} by derivative spectra.

1. Introduction

The spinel supergroup has a complex composition with the general chemical formula AB_2X_4, where A and B are usually divalent and trivalent cations, respectively, and X is an anion. According to the different X anions, it is divided into the oxyspinel group($X = O^{2-}$), thiospinel group($X = S^{2-}$), and selenospinel group($X = Se^{2-}$) [1]. The spinel-type structure can be described as a slightly twisted cubic close-packed array of X anions, with the A and B cations occupying 1/8 of the tetrahedral coordination sites (*T*) and 1/2 of the octahedral coordination sites (*M*), respectively, so that the structure of the oxyspinel group can be described as ${}^{T}A^{M}B_2O_4$. When the B cation is aluminum, it is the aluminum spinel subgroup, in which magnesium and iron ions can be mixed in any proportion. The aluminum spinel subgroup can be further divided by composition: spinel $MgAl_2O_4$, magnesium-iron spinel (Mg, Fe) (Al, Fe)$_2O_4$, hercynite $FeAl_2O_4$, gahnite $ZnAl_2O_4$, galaxite $MnAl_2O_4$, dellagiustaite VAl_2O_4, and thermaerogenite $CuAl_2O_4$.

Gahnite, ideally with the chemical formula $ZnAl_2O_4$, has cubic symmetry and is a less common member of the spinel subgroup. Gahnite is mainly seen in material science studies, but no pure meta gahnite has been observed in nature [2–6], and only a few Zn-rich spinel minerals close to the ideal composition have been reported, and Fe^{2+} substitution, as

well as small amounts of Mg^{2+}, Mn^{2+}, Fe^{3+}, and Cr^{3+}, is also commonly found in samples, with Fe- and Zn-rich spinels commonly appearing as opaque black spinels. Although the chemical composition and petrogenesis of natural spinel [7] and the physical properties of synthetic gahnite [8–10] have been studied extensively by previous authors, systematic analysis of natural gahnite is rare, and its mineralogical and spectroscopic characteristics are rarely reported. Therefore, in this paper, single crystal gahnite from Nigeria was analyzed by basic gemological experiments, electron probe experiments, infrared reflectance spectroscopy, laser Raman spectroscopy, photoluminescence spectroscopy, and UV-VIS spectroscopy to reveal its gemological attribution and spectroscopic characterization.

2. Materials and Methods

2.1. Description of Material. The experimental material of this project is 15 gahnite from Nigeria (see Figure 1), and the sample number is S01~S15. The samples were all produced in the Jemaa region of Nigeria (locally known as Gidan Wiya), where this gem-quality blue octahedral crystal was produced in a complex pegmatite 3.2 km northwest of the site, which is 18 meters wide, trending north-south and surrounded by dark hornblende banded gneiss. Other pegmatites in the area also produce dark green opaque gahnite [11].

2.2. Methods

2.2.1. General Gemological Analysis. A gemological microscope, refractometer, single plate balance (hydrostatic weighing method), UV fluorescent lamp, and Charles filter (CCF) were used to observe the general gemological characteristics of the samples.

2.2.2. Infrared Spectroscopy (FTIR). The samples were tested by infrared spectroscopy using the TENSOR27 Fourier transform infrared spectrometer produced by BRUKER OPTICS, Germany. Test method: reflection method. Test conditions: resolution 8 cm^{-1}, 32 scans, grating setting 6 mm, scanning range 350~4000 cm^{-1}, and scanning speed 10 kHz.

2.2.3. Laser Raman Spectroscopy (RS). LabRAM HR Evolution high-resolution Raman spectrometer from Horiba, France, was used to perform Raman spectroscopy on the samples. Test conditions: excitation light source 532 nm, power 50 mW, confocal pinhole 100, objective 50x, grating inscription density 600 gr·mm^{-1}, measurement range 100~1600 cm^{-1}, acquisition time 12 s, and cumulative times 3; silicon calibration was used before the test.

2.2.4. Photoluminescence (PL). The photoluminescence spectra of the samples were tested using a PL-Image instrument from Biaoqi Optoelectronics Technology Development Corporation (Guangzhou, China). Test conditions: laser light source wavelength 405 nm, integration time 200 ms, average times 20, smoothing width 2, and waveband 420~980 nm.

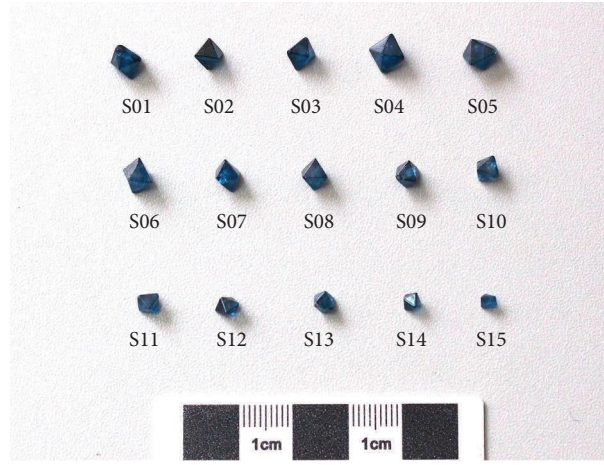

Figure 1: Samples of gahnite from Nigeria.

2.2.5. Ultraviolet-Visible Absorption Spectroscopy (UV-VIS). Ocean Optics GEM-3000 UV-VIS spectrometer was used to test the UV-VIS absorption spectrum of the samples. Test method: reflection method. Test conditions: integration time 120 ms, averaging times 20, smoothing width 5, and waveband 220~980 nm. Data processing: reflectance was converted to absorbance using OPUS software.

The above experiments were done in the gemstone and process materials laboratory at Tongji University.

2.2.6. Electron Microprobe Analysis (EPMA). The electron probe microscopy analyzer type JEOL JXA-8230 of Nippon Electronics Corporation was used to quantitatively analyze the mineral major elements of the sample. Test conditions: accelerating voltage 15 kV, electron beam current 10 nA, and electron beam class diameter 5 μm. Natural and synthetic minerals or oxides are used as standards, and data processing is performed using ZAF correction methods. The experiment was completed at the State Key Laboratory of Marine Geology, Tongji University.

3. Results and Discussion

3.1. Gemological Characteristics. Samples magnified observation of more visible surface triangular etching and triangular growth seats (see Figure 2), refractive index RI 1.792~1.794, a strong vitreous luster, and generally high transparency. Long and short-wave UV fluorescence is inert, with no change under the Charles filter under incandescent light. The specific gravity is 4.45~4.66 (see Table 1).

Comparing the RI value of 1.718 and SG value of 3.06 for common gem-quality magnesia-alumina spinel, it can be found that due to the high zinc content in the mineral, the refractive index and relative density values increase correspondingly with the increase of zinc-to-magnesia-like substitution (zinc atomic mass 65.38 and magnesium atomic mass 24.31).

3.2. Chemical Composition. The chemical composition of 15 gahnite was tested using an electron microprobe, and the results are presented in Table 2.

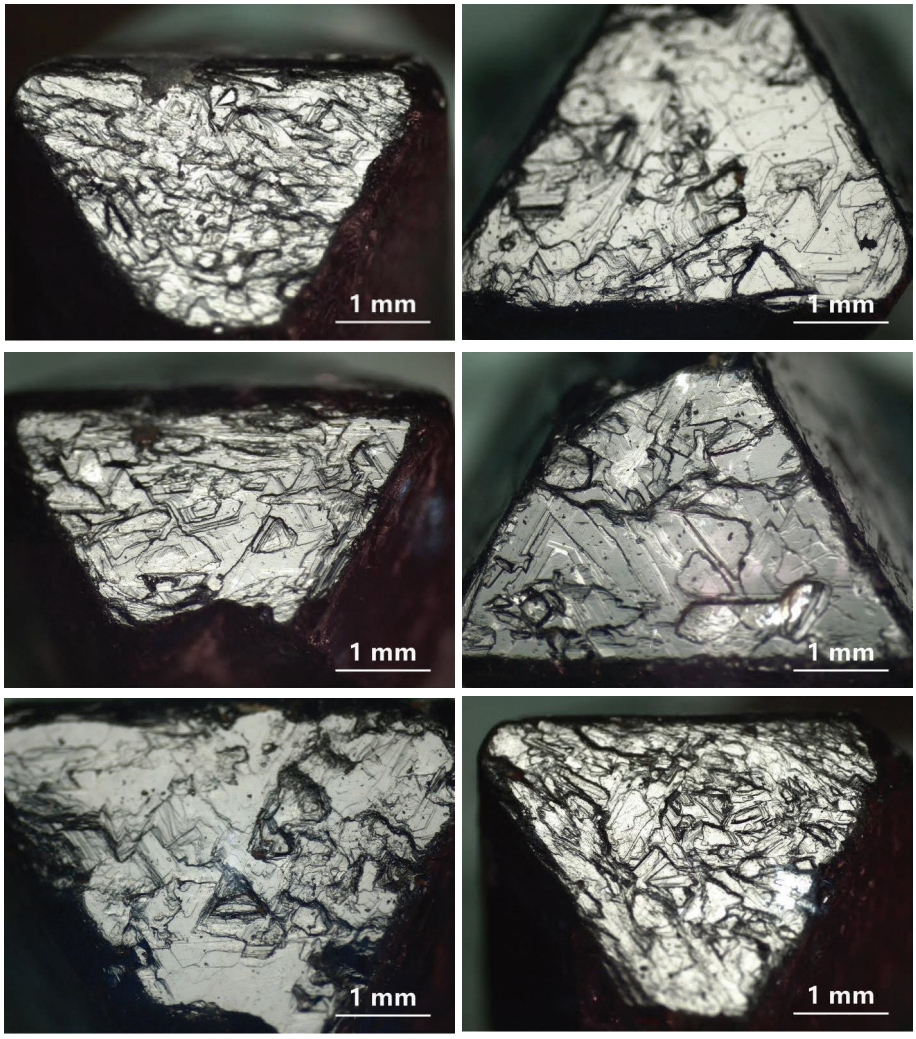

Figure 2: Surface triangular etching and triangular growth seats of gahnite.

Table 1: The gemological characteristics of gahnite.

Samples	RI	Weight		Specific gravity	UV fluorescence	
		Weight (air)	Weight (water)		Long-wave	Short-wave
S01	1.793	0.494	0.387	4.617	Inert	Inert
S02	1.793	0.423	0.330	4.548	Inert	Inert
S03	1.793	0.440	0.343	4.536	Inert	Inert
S04	1.792	0.433	0.337	4.510	Inert	Inert
S05	1.793	0.282	0.219	4.476	Inert	Inert
S06	1.794	0.256	0.198	4.414	Inert	Inert
S07	1.792	0.300	0.235	4.615	Inert	Inert
S08	1.794	0.316	0.247	4.580	Inert	Inert
S09	1.793	0.202	0.157	4.489	Inert	Inert
S10	1.794	0.305	0.238	4.552	Inert	Inert
S11	1.794	0.094	0.073	4.476	Inert	Inert
S12	1.793	0.134	0.105	4.621	Inert	Inert
S13	1.792	0.205	0.159	4.457	Inert	Inert
S14	1.792	0.070	0.055	4.667	Inert	Inert
S15	1.793	0.207	0.161	4.500	Inert	Inert
Average	1.793	0.277	0.216	4.537	Inert	Inert

Table 2: The EPMA test results of gahnite (wt%).

Samples	Al_2O_3	ZnO	FeO	Na_2O	MgO	CoO	MnO	Cr_2O_3	CuO	SiO_2	K_2O	CaO	Total
S01	54.83	40.73	2.37	1.31	0.06	0.02	0.06	0.01	0.00	0.05	0.00	0.00	99.40
S02	56.56	40.23	2.20	1.37	0.05	0.04	0.01	0.00	0.00	0.00	0.00	0.00	100.45
S03	56.13	40.49	2.18	1.32	0.02	0.03	0.02	0.00	0.01	0.00	0.06	0.02	100.20
S04	55.44	40.91	2.24	1.33	0.04	0.05	0.05	0.03	0.01	0.01	0.00	0.00	100.07
S05	55.98	40.72	2.26	1.40	0.05	0.03	0.07	0.04	0.00	0.05	0.00	0.04	100.54
S06	56.06	40.34	2.22	1.32	0.03	0.03	0.09	0.00	0.00	0.03	0.00	0.00	100.10
S07	55.28	40.64	2.16	1.61	0.01	0.10	0.03	0.06	0.07	0.03	0.02	0.00	99.89
S08	55.44	40.48	2.59	1.33	0.04	0.02	0.09	0.02	0.04	0.01	0.00	0.00	100.01
S09	55.14	39.66	2.69	1.33	0.06	0.05	0.02	0.07	0.02	0.01	0.00	0.05	99.02
S10	55.19	40.76	2.00	1.18	0.03	0.05	0.03	0.04	0.00	0.00	0.01	0.00	99.28
S11	55.94	39.74	2.32	1.49	0.00	0.02	0.01	0.03	0.04	0.00	0.03	0.02	99.55
S12	55.55	40.95	2.11	1.27	0.03	0.03	0.03	0.00	0.04	0.02	0.01	0.00	99.97
S13	55.78	40.62	2.31	1.34	0.05	0.07	0.05	0.01	0.00	0.01	0.00	0.01	100.22
S14	55.74	39.48	2.09	1.57	0.03	0.06	0.00	0.03	0.00	0.00	0.01	0.00	99.00
S15	55.47	39.07	3.23	1.30	0.10	0.04	0.05	0.08	0.04	0.02	0.00	0.00	99.34
Average	55.64	40.32	2.33	1.36	0.04	0.04	0.04	0.03	0.02	0.02	0.01	0.01	99.80

The data show that the main chemical composition of the Nigerian gahnite samples is Al_2O_3 and ZnO with an average composition of 55.64% and 40.32%, containing a small amount of FeO with an average composition of 2.33%, in addition to trace amounts of Na, Mg, Co, Mn, Cr, Cu, Si, K, and Ca elements. The chemical formula was calculated to be $Zn_{(0.90)}Fe_{(0.06)}Al_{(1.99)}O_4$, mainly composed of 93.57% $ZnAl_2O_4$, and the other end elements of the aluminum spinel subgroup contained less content, respectively, 6.13% $FeAl_2O_4$, 0.19% $MgAl_2O_4$, and 0.11% $MnAl_2O_4$. Therefore, the gahnite in this experiment belongs to purer gahnite end elements.

3.3. Infrared Spectroscopy. The infrared reflectance spectra of gahnite S01 to S15 were tested, and the results are shown in Figure 3.

The Nigerian gahnite samples all have midinfrared absorption bands near 510 cm^{-1}, 559 cm^{-1}, and 664 cm^{-1}, which are consistent with the infrared spectral characteristics of oxide minerals, showing a small number of wide bands below 800 cm^{-1}. According to the theoretical analysis, the spinel group minerals have four infrared active vibrational peaks, all expressed as T_{1u}, which are called ν_1, ν_2, ν_3, ν_4, according to the frequency. The infrared spectra of the minerals in the group are characterized by two strong and wide absorption bands from 400 to 600 cm^{-1} and two sharp and weak bands below 400 cm^{-1}.

The absorption frequencies of the gahnite samples in this paper were compared with those of the previously studied gahnite (see Table 3). Therefore, the absorptions at 510 cm^{-1} and 559 cm^{-1} shown in this paper belong to the Zn-O stretching vibration and its bending vibration, respectively, which are characteristic absorption peaks of Zn-O. The absorption at 664 cm^{-1} is attributed to the bending vibration of Al-O. Although the absorption peaks in the fingerprint region of 400~1000 cm^{-1} are present in all the spinel group, gahnite is different from natural Mg-Al spinel with absorption peaks at 544 cm^{-1} and 584 cm^{-1} caused by Al-O stretching vibration and 727 cm^{-1} and 845 cm^{-1} caused by Mg-O stretching vibration [13], and these characteristic peaks may be red-shifted with Co^{2+}, Fe^{2+}, and Zn^{2+}-like substitution of Mg^{2+} in the $[MgO_4]$tetrahedra [14].

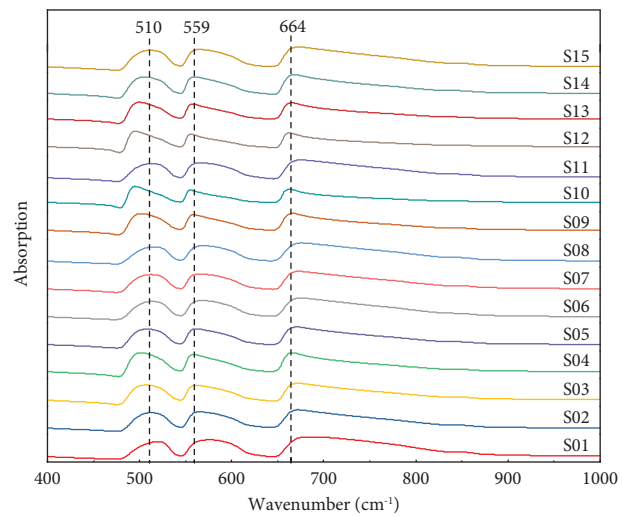

Figure 3: Infrared spectra of gahnite.

Table 3: Infrared spectral absorption wavenumber (cm^{-1}) comparison of gahnite.

T_{1u}	Gahnite This work	Gahnite [6]	Gahnite [12]	Gahnite nanopowder [8]	Assignment
ν_1	510	505	505	498	Zn—O
ν_2	559	550	560	573	Zn—O
ν_3	664	660	665	658	Al—O
ν_4	—	—	745	813	Al—O

3.4. Raman Spectroscopy. The Raman spectra of gahnite S01 to S15 were tested, and the results are shown in Figure 4.

The theory concludes that the simple positive vibrational modes of the general oxide spinel group are $A_{1g} + E_g + 3T_{2g} + 4T_{1u} + T_{1g} + 2A_{2u} + 2E_u + 2T_{2u}$, where $A_{1g} + E_g + 3T_{2g}$ are the five Raman active vibrational mode and $4T_{1u}$ is infrared active. The characteristic absorption peaks of the Raman spectra of Nigerian gahnite show three of the five Raman active modes of the spinel group. The samples all

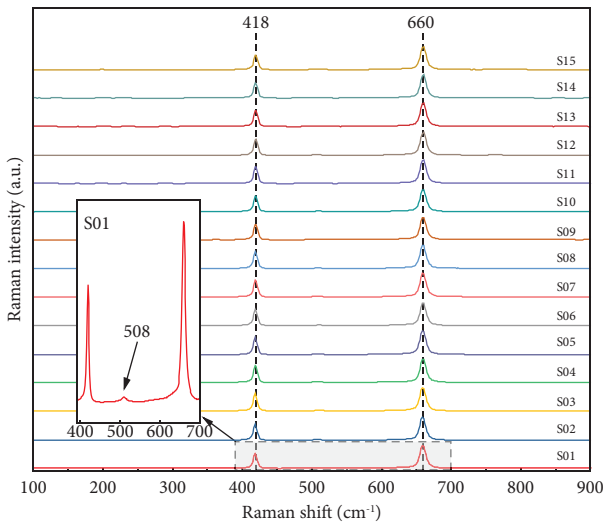

Figure 4: Raman spectra of gahnite.

have characteristic Raman absorption peaks at 418 cm^{-1} and 660 cm^{-1}, corresponding to the E_g mode, high-frequency $T_{2g(3)}$ mode, and another small peak at 508 cm^{-1}, which belongs to the medium-frequency $T_{2g(2)}$ mode. According to previous studies, in the Raman spectrum of $ZnAl_2O_4$, Zn^{2+} mainly acts in the low-frequency part below 250 cm^{-1}, while the part over 250 cm^{-1} is mainly affected by O and Al, and the contribution of O is greater than that of Al [15], so the above characteristic absorption peaks are caused by the Al-O bending vibration of the (AlO_6) octahedron, which belongs to the characteristic Raman spectral peaks of gahnite.

The Raman spectral peak data of gahnite in this work were compared with those of $ZnAl_2O_4$ crystals (theory), natural blue spinel (Fe, Zn chromogenic), natural blue spinel (Co chromogenic), natural pink spinel (Cr chromogenic), and synthetic spinel (see Table 4). As can be seen from the table, although the Raman spectra cannot distinguish between the different colors of spinel, they can effectively spinel and gahnite can be effectively identified among the natural blue spinel. Raman spectroscopy is effective as a means of characterizing the ordered-disordered phase transition of spinel [17]: no 727 cm^{-1} Raman peak for the symmetric stretching vibration attributed to (AlO_4) tetrahedra in gahnite, no structural disorder observed, and no 226 cm^{-1} Raman peak associated with the Mg-Al disorder process as observed in spinel and the N_3 peak 720 cm^{-1} that would strengthen with increasing heating temperature, so the gahnite of this experiment is highly ordered.

3.5. Photoluminescence Spectroscopy. The photoluminescence spectra of gahnite S01 to S15 were tested, and the results are shown in Figure 5.

Five photoluminescence peaks at 675 nm, 686 nm, 698 nm, 708 nm, and 717 nm were present in all the samples in the 650~750 nm band, although there were intensity differences in the fluorescence emission lines of different samples. Grinberg et al. have revealed that lasers of wavelengths less than 600 nm can excite Cr^{3+} ions in the crystal field of spinel-phase strong octahedral crystals [18], which results in five absorptions visible in the 650~750 nm band [19]: (I) 650~680 nm, (II) 680~690 nm, (III) 690~702 nm, (IV) 702~712 nm, and (V) 712~725 nm, which is consistent with the test results in this paper. Electron microprobe analyses showed that the gahnite samples all contained unequal amounts of Cr_2O_3 (Table 2), and thus, the gahnite showed a photoluminescence spectrum that was highly similar to that of the other chromium-doped spinel species [19–21].

Widmer et al. [20] referred to the $^2E \longrightarrow {}^4A_2$ fluorescence emission lines produced by spin-forbidden transitions of Cr^{3+} ions in the spinel structure as R- and N-lines, of which the R-line of the gahnite in the present study is located at 686.3 nm, whereas that of the natural spinel is usually located at 685.6 nm, and the difference in the position of the R-line should be attributed to the differences in the cell parameters of the different spinel species.

Malícková et al. grouped the fluorescence spectra of Cr^{3+} in natural spinel into three categories [19]: (a) purely electronic R-lines, known as the most intense luminescence centers, (b) a series of N-lines associated with eight pairs of Cr^{3+}-Cr^{3+} interactions related to the disruption of short-range ordering of crystals [22], and (c) a series of phonon side bands on the low-energy side of the R-lines (R-PSB), related to the vibrational modes of spinel crystals.

Due to the strong octahedral position preference energy of Cr^{3+}, it is almost certain that in the spinel structure Cr^{3+} ions displace Al only at the octahedral position (*M*), behaving as an ideal [CrO_6] octahedron, i.e., Cr {ideal}, at which point the PL spectra contain only the R-line as well as the R-PSB [21].

In reality, however, Cr^{3+} ions are also present in tetrahedral positions (*T*) causing lattice distortion. The degree of inversion increases, the lower the proportion of Cr {ideal}, the higher the degree of lattice disorder, and the stronger the corresponding N-lines and the weaker the R-lines. The photoluminescence spectra of natural spinel at room temperature in Table 5 show this characteristic of Cr^{3+} ion inversion. The gahnite sample in the II region only sees the obvious and sharp R-line at 686.3 nm, without splitting the N-line, and almost no broadened spectral lines and split peaks. Combined with the Raman spectra, it can be shown that the Zn and Al of the gahnite samples of the present study are almost completely ordered in the *T*-site and *M*-site of the tetrahedral and octahedral coordination.

3.6. Ultraviolet-Visible Absorption Spectroscopy. The wide variety of color variations displayed by the spinel group is due to its structure's ability to accommodate many transition metal cations of different valencies distributed in tetrahedral and octahedral coordination in the spinel structure. The color of spinel is influenced by the element type, valence state, and occupancy, with the color-causing element in blue spinel often thought to be primarily iron or cobalt. The gahnite in this experiment contains FeO and CoO at an average of 2.33% and 0.04%, respectively.

The UV-VIS spectra of gahnite S01 to S15 were tested, and the results are shown in Figure 6.

Table 4: Shift (cm^{-1}) comparison of the spinel Raman mode.

Mode	Gahnite	$ZnAl_2O_4$ crystals	Natural blue spinel (Fe, Zn chromogenic)	Natural blue spinel (Co chromogenic)	Natural pink spinel (Cr chromogenic)	Synthetic spinel
	This work	[15]	[16]	[14]	[17]	[16]
$T_{2g(1)}$	—	194	312	312	312	311
E_g	418	427	406	407	407	402
$T_{2g(2)}$	508	513	—	—	—	—
$T_{2g(3)}$	660	655	664	666	667	673
A_{1g}	—	775	766	767	769	766
Others	—	—	—	—	N_3:720	226, 723

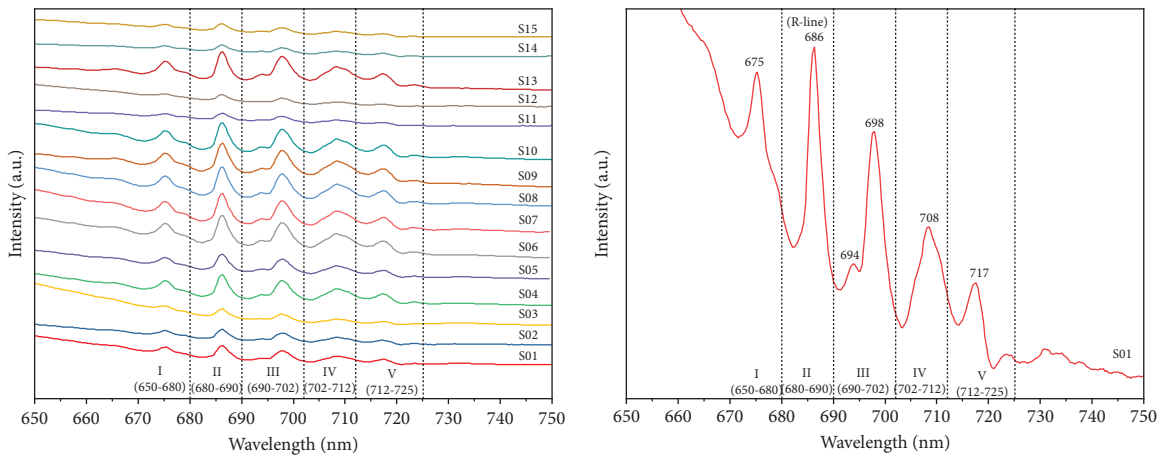

Figure 5: Photoluminescence spectrum of gahnite: (a) S01-S15; (b) S01.

Table 5: Comparison of different Cr^{3+}-activated spinel photoluminescence spectra (650~750 nm) (nm).

Species	650~680	680~690	690~702	702~712	712~725	Source
Natural gahnite	675.3	686.3 (R)	693.8, 697.9	708.5	717.6	This work
Natural spinel	672, 674, 675	685.6 (R), 686, 687, 689	695, 698, 700	705, 707, 709	717, 722	[21]
Natural spinel	677	685 (R)	697	710	718	[19]
Natural spinel	666, 676	686 (R)	698	708	717, 723	[23]
Identification		R/N-line		R-PSB		

The samples all showed absorption bands at 400 nm, 444 nm, 489 nm, and 609 nm, among which 444 nm and 489 nm were the most obvious, which were caused by the *d-d*electron leap of $^{T}Fe^{2+}$ ($^{5}E \longrightarrow {}^{5}T_2$) [19, 24–26], and the absorption band at 400 nm should be due to splitting. The blue-gray hue of the sample is mainly caused by the spin-forbidden electronic transitions in $^{T}Fe^{2+}$ and $^{M}Fe^{2+} \leftrightarrow {}^{M}Fe^{3+}$, and the smaller color saturation of the sample may be due to the lower elemental content of Fe^{2+} and Fe^{3+} [27, 28].

N-order derivative spectra can effectively separate the mutual envelope or overlapping peaks and weak absorption shoulder peaks in the absorption spectrum and give accurate localization and discrimination. The increase of the derivative order resolves the spectrum increase accordingly, but the signal-to-noise ratio decreases. In spectral analysis, the second-order derivative spectrum is the result of the second differentiation of the primary derivative spectrum. It is often used to improve the resolution and accuracy of the raw spectral signal and can produce a sharper response to the nature of the chemical bonds in the sample. Specifically, the second derivative spectrum can help distinguish absorption peaks that are close to the peak top and have similar peak widths, thus improving the resolution of the peaks in the spectrum. To confirm that the weak absorption at 609 nm is related to Co^{2+}, the second-order derivative spectrogram of sample S01 was processed as an example, and the results are shown (see Figure 7). The separation of the weak absorption originally located at 609 nm can be seen by the second-order derivative spectrum showing three absorption peaks at 561 nm, 580 nm, and 609 nm, which are further identified as the typical 500~620 nm Co^{2+} absorption band. It is because Co^{2+} in the T-site in the gahnite tetrahedron permits spin-allowed transitions $^{4}A_2(F) \longrightarrow {}^{4}T_1$ (P) [24, 25]. The latest study demonstrates the effect of Co^{2+} on the color of Nigerian gahnite, explaining the blue-to-green color change process during the heating process [28].

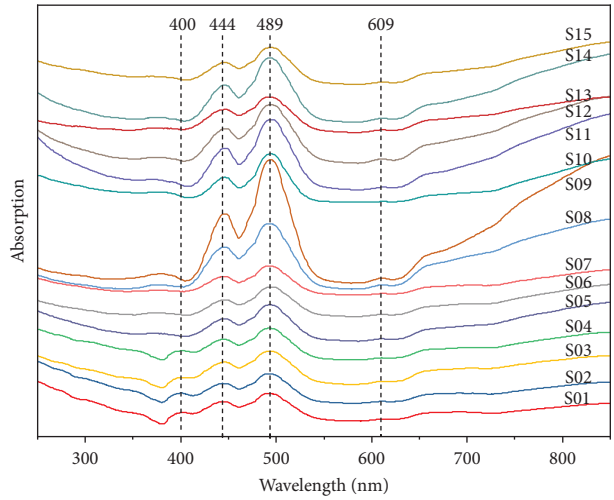

Figure 6: UV-VIS absorption spectrum of gahnite.

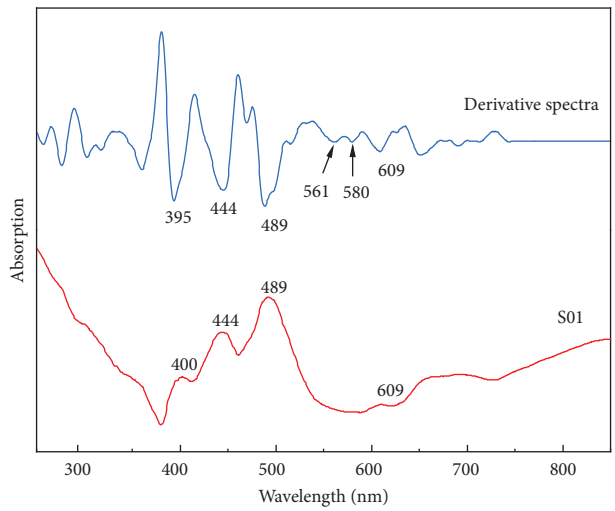

Figure 7: UV-VIS absorption spectrum and derivative spectra of gahnite (S01).

Table 6: UV-VIS spectral absorption bands' comparison of the blue spinel.

Species	Absorption bands	Source
Gahnite	444 nm, 489 nm: *d-d* electron leap of $^{T}Fe^{2+}$ ($^{5}E \longrightarrow {}^{5}T_2$) 609 nm: spin-allowed transitions of $^{T}Co^{2+}$ ($^{4}A_2 \longrightarrow {}^{4}T_1$)	This work
Natural blue spinel (Fe, Zn chromogenic)	458 nm strong absorbent band: characteristic absorption band of Fe 555 nm: related to Fe^{2+}	[24, 25]
Natural blue spinel (Co chromogenic)	300~330 nm: the *d* electron transition of Fe^{3+} ($^{6}A_{1g} \longrightarrow {}^{4}A_{1g}$) 440~430 nm: the outer electron transition of V^{3+} 500~650 nm: areas of concentration of strong and pronounced peaks 595 nm: spin-forbidden transitions of $^{T}Fe^{2+}$ ($^{5}E \longrightarrow {}^{3}T_1$) 550, 585, 625 nm: spin-allowed transitions of $^{T}Co^{2+}$ ($^{4}A_2 \longrightarrow {}^{4}T_1$)	[24, 25]

The positions of the absorption bands of the UV-VIS absorption spectra of gahnite in this work were compared with those of natural blue spinel (Fe, Zn chromogenic) and natural blue spinel (Co chromogenic) compared in this paper (see Table 6). Comparing the natural spinel, the maximum absorption band of $^{T}Fe^{2+}$ of gahnite drifts towards lower energy to 489 nm.

4. Conclusions

Nigerian gahnite samples are granular blue octahedral crystals with refractive indices (RI) of 1.792~1.794, specific gravity (SG) of 4.45~4.66, and no fluorescence. RI and SG values are positively correlated with the degree of homogeneous substitution of zinc for magnesium.

The chemical formula of the Nigerian gahnite sample is $Zn_{(0.90)}Fe_{(0.06)}Al_{(1.99)}O_4$, which mainly consists of 93.57% $ZnAl_2O_4$, and the other end elements of the aluminum spinel subgroup contain fewer components, which are 6.13% $FeAl_2O_4$, 0.19% $MgAl_2O_4$, and 0.11% $MnAl_2O_4$, respectively, belonging to the purer gahnite end elements.

The infrared spectra of the Nigerian gahnite samples showed midinfrared absorption bands near 510 cm^{-1}, 559 cm^{-1}, and 664 cm^{-1} in the fingerprint region all corresponding to Zn-O stretching vibration, bending vibration, and bending vibration of Al-O, respectively. The Raman spectra showed three of the five Raman active modes of the spinel group, with characteristic Raman absorption peaks located at 418 cm^{-1}, 508 cm^{-1}, and 660 cm^{-1}, corresponding to E_g, $T_{2g(2)}$, and $T_{2g(3)}$ modes, respectively, and the higher degree of Zn and Al ordering of Gahnite in this paper was found by comparison. The photoluminescence spectra show the common Cr^{3+}-activated fluorescence splitting peaks of natural spinel, of which the 686 nm (R-line) fluorescence peak is obvious and sharp. The UV-VIS absorption spectra showed absorption bands located at 400 nm, 444 nm, 489 nm, and 609 nm, among which 444 nm and 489 nm were the most obvious, caused by the *d-d* electron leap of $^{T}Fe^{2+}$ ($^5E \longrightarrow {}^5T_2$), and the blue-gray tones of the samples are mainly caused by the spin-forbidden electronic transitions in $^{T}Fe^{2+}$ and $^{M}Fe^{2+} \leftrightarrow {}^{M}Fe^{3+}$; the weak absorption peak at 609 nm was determined to be associated with Co^{2+} by derivative spectra.

Data Availability

The data used to support the findings of this study are included within the article.

Conflicts of Interest

The authors declare that there are no conflicts of interest regarding the publication of this article.

Acknowledgments

This work was supported by the Shanghai Municipal Science Committee (Grant no. 18DZ2281300).

References

[1] F. Bosi, C. Biagioni, and M. Pasero, "Nomenclature and classification of the spinel supergroup," *European Journal of Mineralogy*, vol. 31, no. 1, pp. 183–192, 2019.

[2] S. R. Baswani, B. P. Mishra, S. Mahapatro et al., "Petrochemical evaluation of gahnite from volcanogenic massive sulfide deposits in Betul Belt, central India: insight from petrography and in-situ trace element geochemistry," *Geological Journal*, vol. 57, no. 11, pp. 4508–4528, 2022.

[3] P. Appel, "Gahnite in the ~3.75 Ga isua greens tone belt, west Greenland," *Mineralogical Magazine- Miner Mag*, vol. 64, no. 1, p. 121, 2000.

[4] L. Du, Y. Zhuang, and C. Yang, "Discovery of rhodochrosite and gahnite in the mengjiatun formation, ruxi, China," *Geological Bulletin of China*, vol. 22, no. 1, pp. 65-66, 2003.

[5] Z. Li, W. Zhang, R. Yang, Y. Wen, and W. Zhai, "Electron microprobe compositional analysis of pegmatite beryl melt inclusions and the discovery of gahnite," *Chinese Science Bulletin*, vol. 44, no. 6, pp. 649–652, 1999.

[6] R. Zhang, "Gahnite and lithium phosphomanganese from Altai pegmatites," *Geological Review*, vol. 27, no. 1, pp. 1–7, 1981.

[7] M. M. Phyo, E. Bieler, L. Franz, W. Balmer, and M. S. Krzemnicki, "Spinel from mogok, Myanmar-A detailed inclusion study by Raman microspectroscopy and scanning electron microscopy," *Journal of Gemmology*, vol. 36, no. 5, pp. 418–435, 2019.

[8] B. Goswami and R. Ahlawat, "Impact of annealing on optimization of various thermal, structural, and optical parameters of spinel "gahnite" for device fabrication," *Physica Scripta*, vol. 97, no. 10, Article ID 105808, 2022.

[9] M. Vrankic, B. Grzeta, V. Mandic et al., "Structure, microstructure and photoluminescence of nanocrystalline Ti-doped gahnite," *Journal of Alloys and Compounds*, vol. 543, pp. 213–220, 2012.

[10] Y. D. Ivakin, M. N. Danchevskaya, O. G. Ovchinnikova, and G. P. Muravieva, "Thermovaporous synthesis of fine crystalline gahnite ($ZnAl_2O_4$)," *Journal of Materials Science*, vol. 41, no. 5, pp. 1377–1383, 2006.

[11] B. Jackson, "Gem quality gahnite from Nigeria," *Journal of Gemmology*, vol. 18, no. 4, pp. 265–276, 1982.

[12] W. lu, W. Liang, Z. Zhang, and J. Huang, *Mineral Infrared Spectroscopy*, Chongqing University Press, Chongqing, China, 1988.

[13] H. Shanshan, C. Pan, T. Honglin, and Z. Endong, "Comparative study on spectral characteristics of natural and flame-melting synthetic spinels," *Laser and Optoelectronics Progress*, vol. 58, no. 5, p. 0530001, 2021.

[14] L. Tao, M. Shi, L. Xu, X. Han, and Z. Liu, "Research on spectral characteristics and coloration of natural cobalt spinel," *Spectroscopy and Spectral Analysis*, vol. 42, no. 7, pp. 2130–2134, 2022.

[15] S. López-Moreno, P. Rodríguez-Hernández, A. Muñoz et al., "Lattice dynamics of $ZnAl_2O_4$ and $ZnGa_2O_4$ under high

pressure," *Annalen der Physik*, vol. 523, no. 1–2, pp. 157–167, 2011.

[16] N. Wu, S. Zhang, J. Liu, and Y. Li, "Gemological characteristics of blue spinels colored by different elements," *International Jewelry Academic Exchange Conference Proceedings*, vol. 2021, pp. 121–124, 2021, https://link.cnki.net/doi/10.26914/c.cnkihy.2021.059441.

[17] C. Wang, X. Shen, Y. Liu, and Q. Zhang, "Raman spectra study of heating treatment and order-disorder transition of Cr^{3+}-doped $MgAl_2O_4$ spinel," *Spectroscopy and Spectral Analysis*, vol. 39, no. 1, pp. 109–113, 2019.

[18] M. Grinberg, K. Wisniewski, C. Z. Koepke, D. L. Russell, and K. Holliday, "Luminescence and luminescence kinetics of chromium doped gahnite glass ceramics," *Spectrochimica Acta Part A: Molecular and Biomolecular Spectroscopy*, vol. 54, no. 11, pp. 1735–1739, 1998.

[19] I. Malíčková, P. Bačík, J. Fridrichová et al., "Optical and luminescence spectroscopy of varicolored gem spinel from mogok, Myanmar and Lục yên, vietnam," *Minerals*, vol. 11, pp. 169–172, 2021.

[20] R. Widmer, A.-K. Malsy, and T. Armbruster, "Effects of heat treatment on red gemstone spinel: single-crystal X-ray, Raman, and photoluminescence study," *Physics and Chemistry of Minerals*, vol. 42, no. 4, pp. 251–260, 2015.

[21] Y. Liu, L. Qi, D. Schwarz, and Z. Zhou, "Color mechanism and spectroscopic thermal variation of pink spinel reportedly from kuh-i-lal, Tajikistan," *Gedrag and Gezondheid*, vol. 58, no. 3, pp. 338–353, 2022.

[22] J. Derkosch, W. Mikenda, and A. Preisinger, "N-lines and chromium-pairs in the luminescence spectra of the spinels $ZnAl_2O_4$:Cr^{3+} and $MgAl_2O_4$:Cr^{3+}," *Journal of Solid State Chemistry*, vol. 22, no. 2, pp. 127–133, 1977.

[23] R. L. Mohler and W. B. White, "Influence of structural order on the luminescence of oxide spinels: Cr^{3+}-activated spinels," *Journal of the Electrochemical Society*, vol. 142, no. 11, pp. 3923–3927, 1995.

[24] V. D'Ippolito, G. B. Andreozzi, U. Halenius, H. Skogby, K. Hametner, and D. Günther, "Color mechanisms in spinel: cobalt and iron interplay for the blue color," *Physics and Chemistry of Minerals*, vol. 42, no. 6, pp. 431–439, 2015.

[25] F. Bosi, U. Halenius, V. D'Ippolito, and G. B. Andreozzi, "Blue spinel crystals in the $MgAl_2O_4$-$CoAl_2O_4$ series: Part II. Cation ordering over short-range and long-range scales," *American Mineralogist*, vol. 97, no. 11–12, pp. 1834–1840, 2012.

[26] B. Chauvire, B. Rondeau, E. Fritsch, P. Ressigeac, and J.-L. Devidal, "Blue spinel from the luc yen district of vietnam," *Gems and Gemology*, vol. 51, no. 1, pp. 2–17, 2015.

[27] V. D'Ippolito, G. B. Andreozzi, F. Bosi et al., "Crystallographic and spectroscopic characterization of a natural Zn-rich spinel approaching the endmember gahnite ($ZnAl_2O_4$) composition," *Mineralogical Magazine*, vol. 77, no. 7, pp. 2941–2953, 2013.

[28] T. Stephan, U. Henn, and S. Muller, "On the colour mechanism of blue gahnite from Nigeria," *Journal of Gemmology*, vol. 38, no. 2, pp. 183–193, 2022.